JFET 26(1) (2022) 21-33

Journal of Faculty of Engineering & Technology

journal homepage: www.pu.edu.pk/journals/index.php/jfet/index

Corrosion Study of TiC, TiN, TiAlN, TiO, TiCN PVD Nano-Coatings on AISI 420 JI Surgical Steel

A. Inam*, M. Ishtiaq, M. H. Hassan, I. Ullah, M. K. Saleem, M. Y. Saleem and W. Saleem

Institute of Metallurgy and Materials Engineering, University of the Punjab, Lahore, Pakistan

Abstract

Physical vapor deposition (PVD) coatings are generally applied on surgical implants and cutting tools to increase their service life. The TiN, TiCN, TiC, TiO and TiAlN coatings were deposited by cathodic arc evaporation technique on AISI 420 surgical steel. Various coating parameters i.e., gaseous media, deposition rate and time were studied. Coatings were characterized in terms of surface roughness, adhesion, wear resistance, hardness, and corrosion resistance by surface profilometer, light optical microscopy, nano hardness tester and Gamry potentiostat respectively. Corrosion resistance and biocompatibility of the PVD coatings was determined by cyclic polarization technique in Ringer Lactate media. Surface profile data showed that TiN coating had the lowest value of surface roughness (Ra) while TiO coating showed the highest value of surface roughness. It was revealed from the corrosion test data that TiO coating showed the highest corrosion resistance among all other coatings.

Keywords: Adhesion, Surface Roughness, Corrosion Resistance, Deposition, Ringer Lactate.

1. Introduction

Martensitic stainless steels are promising materials in surgical tools due to their high resistance to wear, corrosion and ease of fabrication [1-3]. These steels may corrode when exposed to gaseous or aqueous environments, in this regard the extent of corrosion is evaluated in relation to protective coatings and the aggressiveness of environment [4-7]. In view of surgical applications, they are susceptible to localized corrosion in body fluids due to surface/tissue interaction at the interface [8, 9]. During interaction between metallic devices and living tissues (including blood and arterial tissues) durability and safe usage largely depends upon the surface properties of the metallic tools. The surface properties of surgical steels can be improved by deposition of suitable biocompatible materials by various coating techniques and it has become an intriguing area of research [10-26]. The thin film coatings of titanium compounds exhibit high wear resistance, good adhesion, and excellent biocompatibility with good chemical stability [27-31].

Numerous studies on applying Ti coatings with addition of multiple elements have made it possible to increase the tool service life with high corrosion resistance and improved mechanical properties through surface modification [32-36]. Different physical vapor deposition (PVD) techniques were adopted to achieve required composition of coating layer [37, 38]. During the PVD, macro-particles may generate due to the cathode deposition as

* Corresponding Author: aqil.imme@pu.edu.pk

swollen regions on the coating surface. Due to potential difference these regions are more liable to the localized corrosion. Other than PVD, cathodic arc deposition (CAD) is noteworthy owing to obtain the dense structure, high deposition rate and low processing temperature [39, 40]. Due to growing interest in various applications of TiN, TiCN, TiC, TiO and TiAlN in surgical and biomedical field, the functionality of bulk surfaces, corrosion resistance and mechanical properties has been studied by various researchers [39-44]. However, a comparative study in terms of biocompatibility and adhesion strength of all these coatings was still missing which has been addressed in this study.

The aim of this study is to evaluate the effect of TiC, TiO, TiN, TiAlN and TiCN nano-coatings on micro-hardness and degree of adhesion deposited on AISI 420 J1 stainless steel substrate by cathodic arc deposition. The corrosion behaviour of titanium coatings as a function of different chemical composition was investigated in ringer lactate solution (body simulated fluid) to determine the bio compatibility.growth in the supply side[7]. In 2016 the electricity demand-supply gap was 31.6 TWh annually which led to 2.5% decrease in GDP and more than 0.5 million unemployment in the industrialized sector [8].

2. Materials and Methods

2.1. Materials

For the present study, a commercial grade martensitic stainless steel AISI 420 J1 was selected.

2.2. Cathodic arc evaporation/ deposition

After doing fine grinding, prior to coating process, the substrate of AISI 420-J1 steel was rinsed with trichloroethylene and deionized to ensure the cleanness. For the deposition of TiO, TiC, TiN, AlTiN and TiCN coatings, the substrate was loaded into the chamber of vacuum ion plating machine. Before coatings, the specimens were bombarded with argon (Ar+) at 7.4 x 10-1 Pa pressure to get good adhesion. Reactive gas nitrogen was fed to the chamber for nitride coatings. During the deposition the current and voltage were maintained at 50-70A and 600-800 V respectively. The coating codes and colour of coatings are given in table 1.

2.3. Scanning Electron Microscopy

Scanning electron microscopy including SEs imaging and EDX analysis was carried out on FEI Inspect S50 SEM equipped with new generation EDX Silicon Drift Detector.

2.4. Profilometery

The surface topography of the coated substrate was analyzed using contact profilometer with diamond stylus. The stylus scanned the coated surface vertically and laterally and recorded different surface roughness parameters as given in Table 2.

2.5. Scratch test

Scratch test was performed using micro-scratch tester with diamond indenter (100 micron radius). The initial and end loads applied were 0.03 N and 20 N respectively with loading rate of 9.99 N/min while the acoustic emission sensitivity was adjusted at 7.

2.6. Hardness test

Hardness was obtained by using micro-Vickers hardness tester (Vision Vubeit China 402 ND) with a diamond indenter (Berkovich BJ-48) in accordance to the rules of Oliver and

Pharr (O & P). The load exerted/employed during indentation was 50 mN with 100 mN/min loading and unloading rates. The holding time was 20s.

2.7. Adhesion testing

Adhesion test was carried out according to the standard VDI 3198 by using Rockwell nano-hardness tester. A diamond indenter was utilized to penetrate through coatings and the images of indents were adequately analysed using conventional light optical metallurgical microscope. The patterns of cracks were validated by comparing with the standard VDI 3198.

2.8. Electrochemical studies

For electrochemical testing, 1cm2 coated specimens of AISI 420 J1 stainless steel were rinsed with deionized water. Ringer lactate solution (body simulated fluid) was used as an electrolyte. The corrosion behaviour was analysed by electrochemical technique i.e., cyclic polarization using Gammry Potentiostate PC14/750 and Echem analyst version 5.68 for spectrum study. The test was performed using three electrode system; PVD coated AISI 420 J1 martensitic stainless steel (MSS) specimen as working electrode, saturated calomel electrode (SCE) and graphite as reference and auxiliary electrodes respectively. Open circuit potential (OCP) was measured for 600 s with 0 mV.s-1 stability. To evaluate the pitting susceptibility of the PVD coated AISI 420 J1 MSS, the cyclic polarization scan was obtained by polarizing the surface between -500 mV and 300 mV versus OCP respectively with apex current density of 10 mA /cm2. Apex potential of 1500mV versus OCP was adjusted with a rate of 5 mV.s-1 and 2.5 mV.s-1 for forward and reverse polarization scans, respectively.

3. Results and Discussion

3.1. Scanning Electron Microscopy

Different colours of coating on AISI AISI 420 J1 martensitic stainless steel were obtained as the result of cathodic arc evaporation technique which are given in Table 1.

Table 1. Codes and colours of TiO, TiCN, TiAlN, and TiN coatings.

Coating Code	Coatings	Color
M-1	TiO	Rainbow
RG-1	TiCN	Rose Gold
BL-1	TiO	Blue
P-1	TiO	Purple
B-1	TiAlN	Black
B-2	TiAlN	Purple
G-1	TiN	Gold

EDX spectrum and composition of TiN coating is shown in Figure 1. Titanium and nitrogen peaks are clearly visible in the EDX spectrum and are confirming TiN coating. In the electron image, coating is intact very much with the base 420 J1 steel confirming a good adhesion (Figure 2).

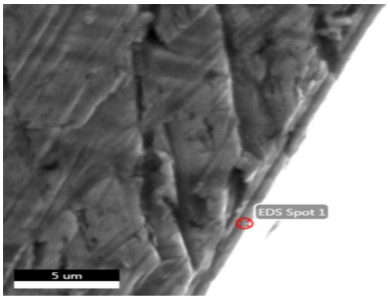

Element	Weight %
C K	11.96
N K	12.77
SiK	3.23
TiK	23.49
CrK	6.48
FeK	42.07

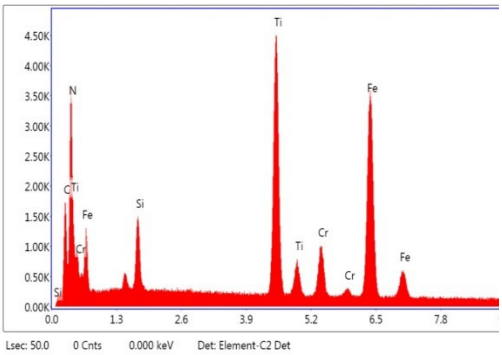

Figure 1: EDX spectrum and composition analysis of the TiN coating over 420 J1 steel.

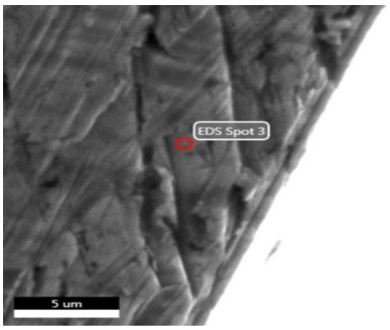

Element	Weight
C K	12.52
SiK	1.84
CrK	10.45
FeK	75.18

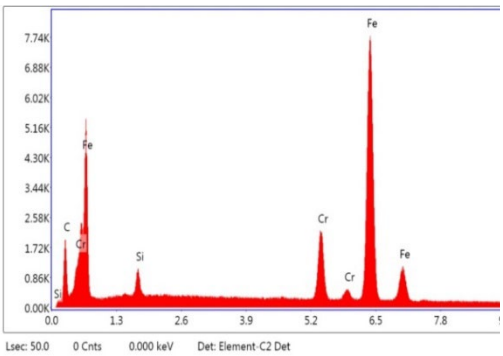

Figure 2: EDX spectrum and composition analysis of the base 420 J1 steel on which TiN coating was applied.

3.2. Hardness testing

The variation in the hardness of the deposited coating with varying indentation load is shown in Figure 3. The micro-hardness variation trend is similar to as reported in a study [14]. The curve does not follow the path of loading when the load is released. The behaviour is attributed to ductile materials. The micrograph of the indent depicting the ductile behaviour of coating is shown in Figure 4.

3.3. Adhesion testing

Colourful coatings were obtained by PVD on AISI 420 J1 substrate apparently with no macroscopic imperfections. The micrographs of Berkovich diamond indentation on substrate surface are shown in Figures 5-7 reveal the adhesion quality of coatings. Bulging and localized chipping of the coating substrate surface was examined in the indentation area.

Comparing with the standard VDI 3198 it comes to light that the high ductility (low hardness) of the coatings led to the vicious delimitation which indicate the adverse adhesion at coating substrate interfaces.

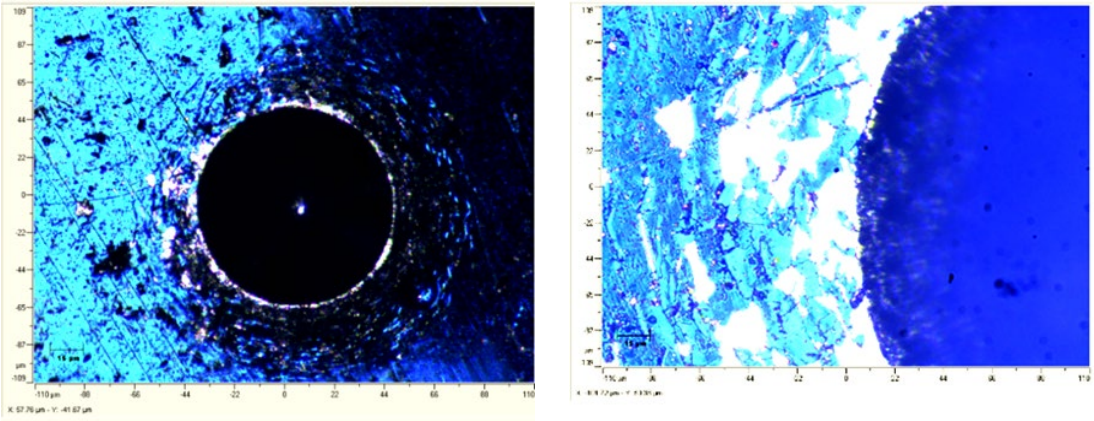

Figure 3: Micrograph of Berkovich diamond indentation on the surface of AISI 420 J1 (BI-1) with TiO coating: (a) micro-fractures around the indentation edge (b) spherical section within the indentation revealing fracture propagation in the coating.

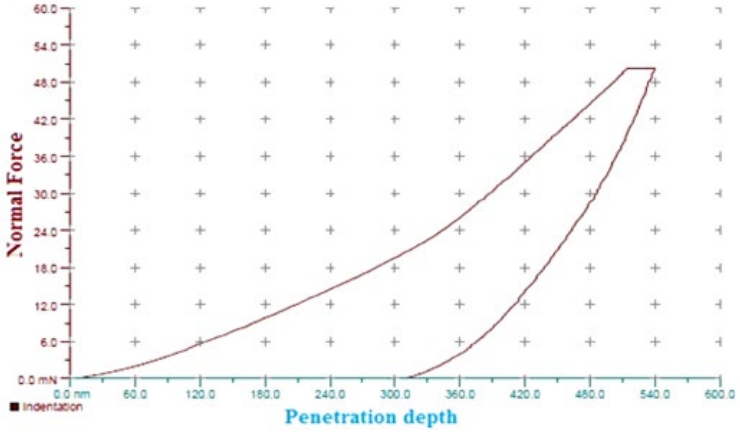

Figure 4: A plot of normal force vs penetration depth by micro-vickers hardness tester with a Berkovich BJ-48 diamond indenter.

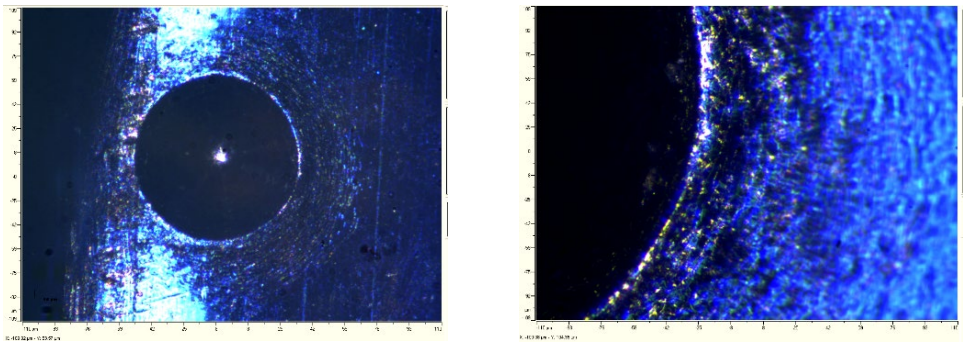

Figure. 5: Micrograph of Berkovich diamond indentation on the surface of AISI 420 J1 (BI-1) with TiO coating: (a) micro-fractures around the indentation edge (b) spherical section within the indentation revealing fracture propagation in the coating.

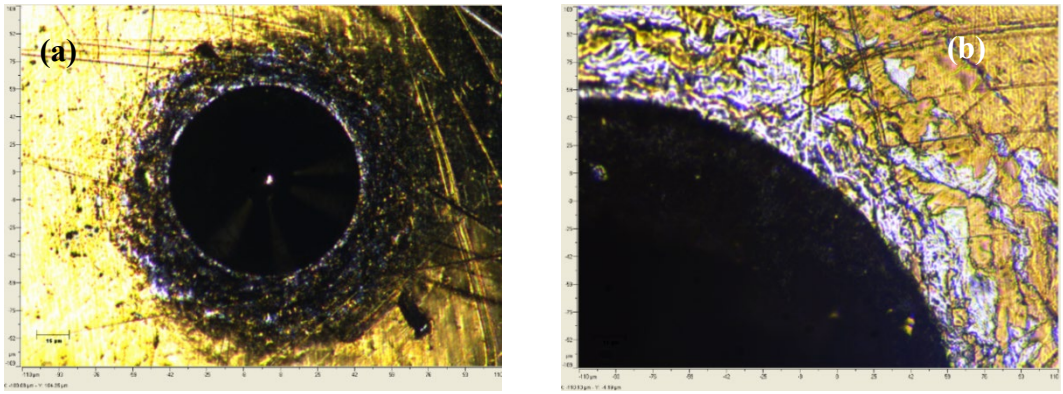

Figure 6: Micrograph of Berkovich diamond indentation on the surface of AISI 420 J1 (B-1) with TiAlN coating: (a) micro-fractures around the indentation edge (b) spherical section within the indentation revealing fracture propagation in the coating.

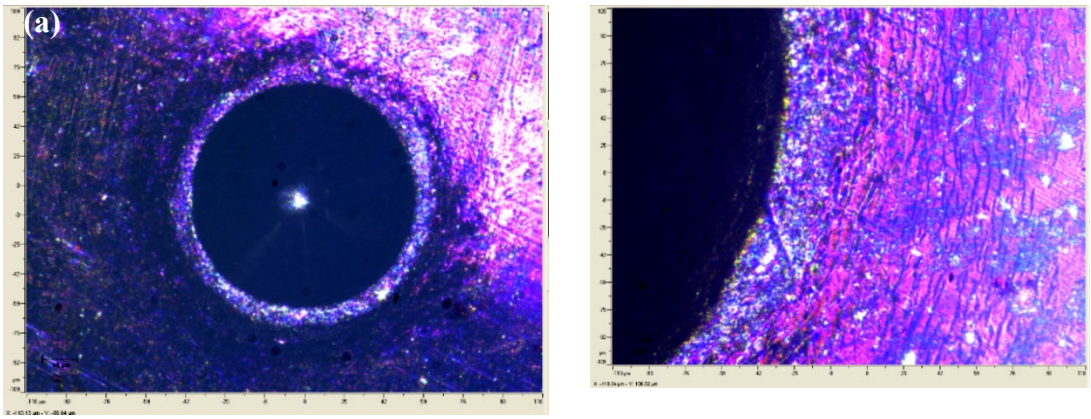

Figure 7: Micrograph of Berkovich diamond indentation on the surface of AISI 420 J1 (B-2) with TiAlN coating: (a) micro-fractures around the indentation edge (b) spherical section within the indentation revealing fracture propagation in the coating.

3.4. Scratch Test

Acoustic emission

The graph of acoustic emission of the coating is shown in Figure 8. The straight-line graph reveals that there are no crack imitation and growth regions in the indentation periphery. This result is in good agreement with hardness and adhesion testing results, where the coating piled up instead of tearing due to its high ductility/softness. The penetration depth was more than 359900 nm depicting low mechanical adhesion between coating and substrate as shown in Figure 9. The comparison between the critical load and the hardness of the coating shows that an increase in load results the decrease in micro hardness as well as mechanical adhesion of coating.

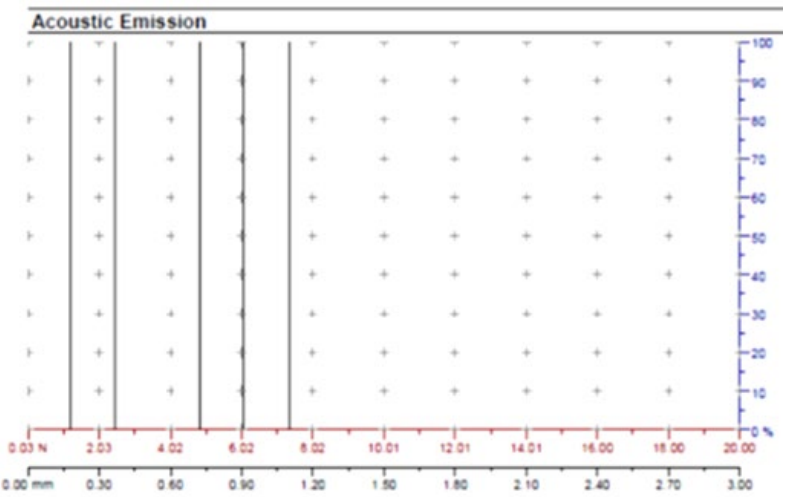

Figure 8: Acoustic emission curves produced during the scratch placed by utilizing Rockwell nano hardness tester at sensitivity level 7.

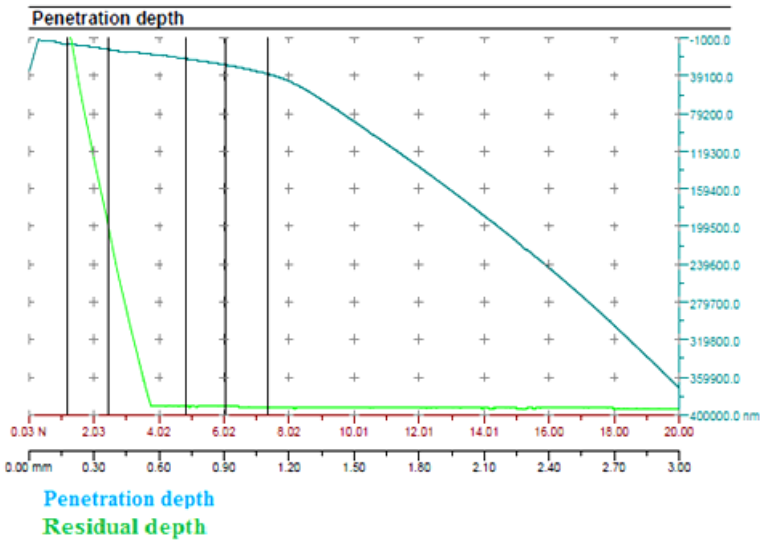

Figure 9: A plot of penetration depth (nm) Vs normal force (N) during the scratch placed by utilizing Rockwell nano hardness tester.

In this crack test, delamination of coating was observed and is shown in Figure 10 (a, b, c) while at higher critical load the coating piled up due to increase of substrate contribution as revealed in Figure 10 (d, e).

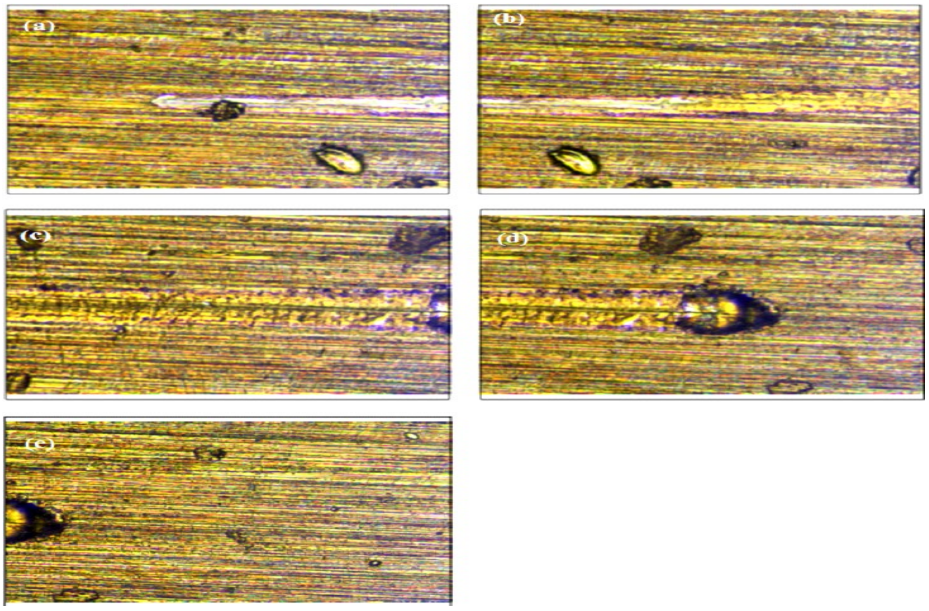

Figure 10: Illustration of scratch progress at; (a) Critical load (Lc 1) is 1.2 N (b) Critical load (Lc 2) is 2.48 N, (c) Critical load (Lc 3) is 4.85 N, (d) Critical load (Lc 4) is 6.06 N, (e) Critical load (Lc 5) is 7.36 N.

3.5. Profilometry

Graphically, the average roughness is the area between the roughness profile and its central line divided by the evaluation length (normally five sample lengths with each sample length equal to one cut off). Surface parameters of different coatings are given in Table 2.

Descending order of surface roughness of deposited coatings is given as;

G-1 > RG-1 B-2> BL-1> B-1 > P-1> M-1

Table 2. Surface roughness values of different coatings.

Sample	Ra	Rz	Rq	Rt	Rp
BL-1	0.27	2.70	0.36	4.97	1.92
RG-1	0.23	2.42	0.29	3.31	1.69
B-2	0.26	1.84	0.32	4.44	1.04
G-1	0.12	1.00	0.15	2.03	0.43
P-1	0.32	2.14	0.39	3.38	1.35
B-1	0.30	2.89	0.41	4.75	1.91
M-1/TiO-4	0.33	3.77	0.47	7.94	1.88

3.6. Corrosion testing

The cyclic polarization curves for TiO, AlTiN and TiN coatings on AISI 420 J1 in ringer lactate solution are shown in Figure 11.

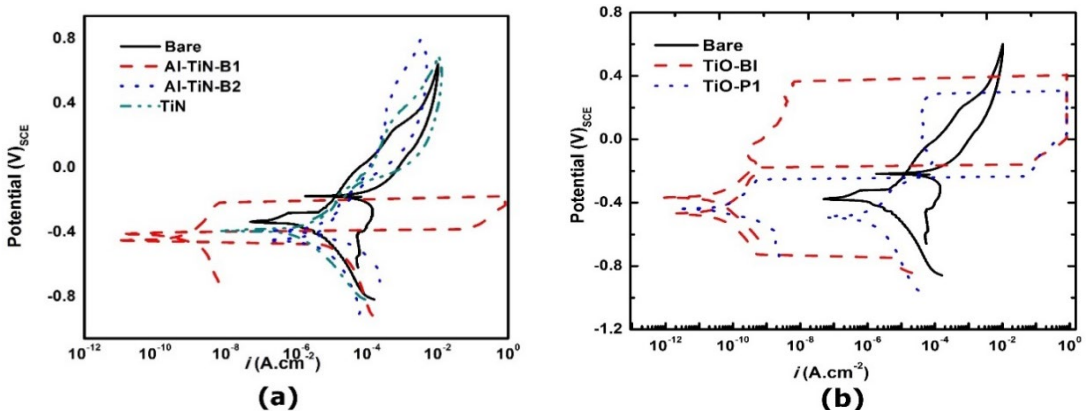

Figure 11: Cyclic polarization scans of AISI 420 J1 in ringer lactate solution (a) TiN, AlTiN (b) TiO.

The cyclic polarization curves depict the preferential dissolution tendency of coatings in ringer lactate solution which incorporates the cathodic polarization, Tafel region and passive region followed by the reverse scan.

In Figure11 (a), a small positive hysteresis loop by reverse polarization was observed due to the localized attack on the surfaces of TiN and AlTiN-B2 coatings on steel substrate by aggressive chloride and bicarbonate ions present in the ringer lactate solution. The increment in corrosion current density icorr for AlTiN-B1 was attributed to the continuous pits initiation process due to discrepancies in the coated surface. The small hysteresis loop in case of TiN indicated the less corrosion tendency and its protection potential (Eprot) was nobler (-262.9 mV) than that of ALTiN (-436.3 mV) coating. The active potential (more negative) was monitored for ALTiN coatings with higher corrosion current density (icorr) and less difference in the break down potential (Ebd) and Eprot due to localized electrochemical reactions by carbonate and chloride (Cl-) ions with the coating and underlying metal as delamination of the coating occurred as shown in Table 3.

However, the highest difference between E_{bd} and E_{prot} was observed for TiN with low current density resulted low corrosion rate (0.036 mpy) than for AlTiN coating (2.175 mpy).

Table 3. Electrochemical parameters of cyclic polarization scan for coatings.

Sample ID	E_{corr1} (mV)	E_{corr2} (mV)	E_{bd} (mV)	E_{prot} (mV)
TiO (P1)	-490.3	-437.9	287.1	-241.1
TiO (BL-1)	-467.7	-367.9	365.9	-148.3
TiN	-432.8	-357	627	-262.9
AlTiN (B1)	-491.1	-451.8	-257.3	-436.3
AlTiN (B2)	-491.7	-431.8	347.2	-322.2

Table 4. Electrochemical parameters of cyclic polarization in the tafel region.

Sample	E_{ocp} (mV)	i_{corr} (A.cm^{-2})	E_{corr} (mV)	Corrosion Rate (mpy)	R_p (Ω.m^2)
Bare	-363.9	254×10^{-6}	-216	111.4	347
TiO-P	-456.3	1.2×10^{-6}	-492	0.5313	40753
TiO-BL	-343	57×10^{-12}	-367	0.025×10^{-3}	948366339
TiN	-357	57×10^{-9}	-431.0	0.036	125887
AlTiN-B1	-457.3	2.16×10^{-6}	-469	0.8978	19772
AlTiO-B2	-447	4.9×10^{-6}	-431	2.175	8003

Cyclic polarization scans for TiO coated 420 J1 Stainless steel are shown in Figure 11 (b). The shift of the anodic polarization curves towards the right side than that of the bare metal reveals the passivation on the coated surface comparative to bare metal. The nobler potential (less negative) was recorded for TiO-BI coated 420 J1 SS ascribing low corrosion rate (0.025 mpy) and least corrosion current density (Table 4). The break down potential (Ebd) of TiO coatings were much positive (365 mV) than the Ebd of AlTiN (-257.2 mV) that depicted the corrosion resistance tendency of TiO coatings is more prominent [15]. In case of TiO-BI, protection potential (-148.3 mV) was more positive than the corrosion potential (-467.7mV) that indicates the surface was quite resistant to pitting and only existing pits grew (Table 3). The rapid increase in corrosion current density above the Ebd is attributed to the pit formation process while the shift is the result of passive film formed on the surface.

The polarization resistance of coated surface was calculated by using formula (equation 1)

$$R_p = \frac{\beta_a \beta_c}{2.3\,(\beta_a+\beta_c) i_{corr}} \qquad (1)$$

Where anodic (βa), cathodic (βc) are Tafel slopes in (mV/decade) and corrosion current density (icorr) in A.m-2 got by extrapolating Tafel regime on cyclic polarization scan values given in Table 4.

The high resistance polarization (Rp) was found in case of TiO-BI and TiN indicating the formation of passive film and retarding the corrosion phenomena on surface. While lowest resistance to polarization was observed on bare steel surface with highest corrosion rate (111.4 myp) and low polarization resistance in AlTiN is indication of dissolution of coating in ringer lactate solution which supports breakdown potential results as shown in Table 4.

4. Conclusions

Following conclusions are drawn from this study:

- Uni. and multi-coloured coatings were successfully deposited by Cathodic Arc Evaporation (CAE) on AISI 420 J1 martensitic stainless steel.
- The TiO and TiN coatings showed comparatively more corrosion resistance by forming passive film on the surface with the solution ions (Cl^-, CO_3^{-2})

- The TiO, TiN and AlTiN coatings were ductile rather than brittle; no cracks were found, imputing low hardness.
- The TiO, TiN coated AISI 420J1 martensitic stainless steel can be used in surgical tools with little improvement in its adhesion.

References

[1]. V. Geantă, et al, "Stainless Steels with Biocompatible Properties for Medical Devices," Key Eng Mater, 583 (2014), 9-15.

[2]. A.J. Sedriks, "Corrosion of stainless steel," 2. 1996.

[3]. B. Rosborg, and A. Rosengren, "Slow strain rate testing of an austenitic stainless steel under electrochemical control in high temperature water", Corros Sci, 20 (2) (1980), 301-306.

[4]. X.W. Lei, et al, "Investigation of stress corrosion cracking behavior of super 13Cr tubing by full-scale tubular goods corrosion test system", Eng Fail Anal, 50 (2015), 62-70.

[5]. Y. Zhao, et al, "Pourbaix diagram for HP-13Cr stainless steel in the aggressive oilfield environment characterized by high temperature, high CO_2 partial pressure and high salinity", Electrochim Acta, 293 (2019), 116-127.

[6]. X. Lei, et al, "Impact of reversed austenite on the pitting corrosion behavior of super 13Cr martensitic stainless steel", Electrochim Acta, 191 (2016), 640-650.

[7]. T. Sunaba, et al., "Influence of chloride ions on corrosion of modified martensitic stainless steels at high temperatures under a CO_2 environment", Corros, 70(10) (2014), 988-999.

[8]. K. Nielsen, "Corrosion of metallic implants", Br Corros J 22 (4) (1987) 272-278.

[9]. I. Gurappa, "Characterization of different materials for corrosion resistance under simulated body fluid conditions", Mater Charact, 49 (1) (2002), 73-79.

[10]. A. Inam, et al., "Effect of voltage and spray–off distance of electric-arc spray technique on surface properties of nickel–chrome (Ni–Cr) coating developed on 304L stainless steel", Mater Res Express, 7 (1) (2020), 016525.

[11]. W. Fredriksson, et al., "Full depth profile of passive films on 316L stainless steel based on high resolution HAXPES in combination with ARXPS", Appl Surf Sci, 258 (15) (2012), 5790-5797.

[12]. B. Zhang et al., "Unmasking chloride attack on the passive film of metals", *Nat commun*, 9 Article number: 2559 (2018), 1-9.

[13]. J. Soltis, "Passivity breakdown, pit initiation and propagation of pits in metallic materials–review", Corros Sci, 90 (2015), 5-22.

[14]. L. Liu, Y. Li, and F. Wang, "Influence of nanocrystallization on passive behavior of Ni-based superalloy in acidic solutions", Electrochim Acta, 52 (7) (2007) 2392-2400.

[15]. L. Liu, Y. Li, and F. Wang, "Influence of grain size on the corrosion behavior of a Ni-based superalloy nanocrystalline coating in NaCl acidic solution", Electrochim Acta, 53 (5) (2008), 2453-2462.

[16]. T. Li, et al, "An investigation on the continuous and uniform thin membrane passive film formed on sputtered nanocrystalline stainless steel", Corros Sci, 104 (2016),71-83.

[17]. N. Lin, et al, "Comparison of surface fractal dimensions of chromizing coating and P110 steel for corrosion resistance estimation", Appl Surf Sci, 311 (2014), 330-338.

[18]. J. Högström, et al, "Cation profiling of passive films on stainless steel formed in sulphuric and acetic acid by deconvolution of angle-resolved X-ray photoelectron spectra", Appl Surf Sci, 284 (2013), 700-714.

[19]. B. Zhang, et al, "Quasi-in-situ observing the growth of native oxide film on the FeCr15Ni15 austenitic alloy by TEM", Corros Sci, 140 (2018), 1-7.

[20]. C. Pan, et al, "The electrochemical corrosion behavior of nanocrystalline 304 stainless steel prepared by magnetron sputte*ring*", J Electrochem Soc, 159 (11) (2012), C453.

[21]. N. E. Hakiki, et al, "Semiconducting properties of passive films formed on stainless steels: influence of the alloying elements", J Electrochem Soc, 145 (11) (1998) 3821.

[22]. E. Hamada, et al, "Direct imaging of native passive film on stainless steel by aberration corrected STEM", Corros Sci, 52 (12) (2010), 3851-3854.

[23]. H. J. Jang, and H. S. Kwon, "In situ study on the effects of Ni and Mo on the passive film formed on Fe–20Cr alloys by photoelectrochemical and Mott–Schottky techniques*",* J Electroanal Chem, 590 (2) (2006), 120-125.

[24]. A. Fattah-Alhosseini, et al, "The semiconducting properties of passive films formed on AISI 316 L and AISI 321 stainless steels: A test of the point defect model (PDM)", Corros Sci, 53 (10) (2011), 3186-3192.

[25]. S. Ningshen, et al, "Semiconducting and passive film properties of nitrogen-containing type 316LN stainless steel*s*", Corros Sci, 49 (2) (2007), 481-496.

[26]. H. X. Guo, B.T. Lu, and J.L. Luo, "Study on passivation and erosion-enhanced corrosion resistance by Mott-Schottky analysis*",* Electrochim acta, 52 (3) (2006), 1108-1116.

[27]. J.G. Han, et al, "High temperature wear resistance of (TiAl)N films synthesized by cathodic arc plasma deposition*",* Surf Coat Technol, 86-87 (1996), 82-87.

[28]. B.F. Coll, et al, "*(TiAl)N advanced films prepared by arc process"*, Mater Sci Eng. A, 140 (1991), 816-824.

[29]. D.Y. Wang, et al, "Improvement of the interfacial integrity of (TiAl)N hard coatings deposited on high speed steel cutting tools", Surf Coat Technol, 120-121 (1999), 388-394.

[30]. T. Suzuki, D. Huang, and Y. Ikuhara, "Microstructures and grain boundaries of (TiAl)N films", Surf Coat Technol, 107 (1) (1998), 41-47.

[31]. J.R. Roos, et al, "Interrelationship between processing, coatingproperties and functional properties of steered arc physically vapour deposited (Ti,Al)N and (TiNb)N coatings", Thin Solid Films, 193-194 (1990), 547-556.

[32]. J.G. Han, K.H. Nam, and I.S. Choi, "The shear impact wear behavior of Ti compound coatings", Wear, 214 (1) (1998), 91-97.

[33]. K.-L. Lin, M.-Y. Hwang, and C.-D. Wu, "The deposition and wear properties of cathodic arc plasma deposition TiAlN deposits", Mater Chem Phys, 46 (1) (1996), 77-83.

[34]. A. Kimura, et al, "Hot-pressed Ti-Al targets for synthesizing Ti1−xAlxN films by the arc ion plating method", Thin Solid Films, 382 (1) (2001), 101-105.

[35]. P.C. Jindal, et al, "Performance of PVD TiN, TiCN, and TiAlN coated cemented carbide tools in turning", Int J Refract Hard Met, 17 (1) (1999),163-170.

[36]. H.G. Prengel, et al, "Advanced PVD-TiAlN coatings on carbide and cermet cutting tools", Surface and Coatings Technology, 94-95 (1997), 597-602.

[37]. L. Shan, et al, "Tribological behaviours of PVD TiN and TiCN coatings in artificial seawater", Surf Coat Technol, 226 (2013), 40-50.

[38]. G. Cassar, et al, "Impact wear resistance of plasma diffusion treated and duplex treated/PVD-coated Ti–6Al–4V alloy", Surf Coat Technol, 206 (10) (2012), 2645-2654.

[39]. R.P. van Hove, et al, "Titanium-nitride coating of orthopaedic implants: a review of the literature*",* BioMed Res Int, 2015. 2015.

[40]. I. Gotman, and E.Y. Gutmanas, "Titanium nitride-based coatings on implantable medical devices*",* Advanced Biomaterials and Devices in Medicine, 1 (1) (2014), 53-73.

[41]. H.A. Ching, et al, "Effects of surface coating on reducing friction and wear of orthopaedic implants*",* Sci Technol Adv Mate, 15 (1) (2014), 014402.

[42]. M.T. Raimondi, and R. Pietrabissa, "The in-vivo wear performance of prosthetic femoral heads with titanium nitride coating", Biomaterials, 21 (9) (2000), 907-913.

[43]. S. Piscanec, et al, "*Bioactivity of TiN-coated titanium implants*", Acta Mater, 52 (5) (2004), 1237-1245.

[44]. A.P. Serro, et al, "*A comparative study of titanium nitrides, TiN, TiNbN and TiCN, as coatings for biomedical applications*", Surf Coat Technol, 203 (24) (2009), 3701-3707.